September, 2005

Phase error compensation for a 3-D shape measurement system based on the phase-shifting method

Song Zhang, *Harvard University*
Peisen S. Huang, *State University of New York at Stony Brook*

Phase Error Compensation for a 3-D Shape Measurement System Based on the Phase-Shifting Method

Song Zhang[a] and Peisen S. Huang[b]

[a] Department of Mathematics, Harvard University, Cambridge, MA 02138, Email: {szhang}@fas.harvard.edu
[b] Department of Mechanical Engineering, SUNY at Stony Brook, Stony Brook, NY 11794-2300, Email: {peisen.huang}@stonybrook.edu

ABSTRACT

This paper describes a novel phase error compensation method for reducing the measurement error caused by non-sinusoidal waveforms in the phase-shifting method. For 3D shape measurement systems using commercial video projectors, the non-sinusoidal nature of the projected fringe patterns as a result of the nonlinear gamma curve of the projectors causes significant phase measurement error and therefore shape measurement error. The proposed phase error compensation method is based on our finding that the phase error due to the non-sinusoidal waveform of the fringe patterns depends only on the nonlinearity of the projector's gamma curve. Therefore, if the projector's gamma curve is calibrated and the phase error due to the nonlinearity of the gamma curve is calculated, a look-up-table (LUT) that stores the phase error can be constructed for error compensation. Our experimental results demonstrate that by using the proposed method, the measurement error can be reduced by 10 times. In addition to phase error compensation, a similar method is also proposed to correct the non-sinusoidality of the fringe patterns for the purpose of generating a more accurate flat image of the object for texture mapping. While not relevant to applications in metrology, texture mapping is important for applications in computer vision and computer graphics.

Keywords: 3-D shape measurement, phase-shifting, non-sinusoidal waveform, phase error compensation, projector, gamma curve, look-up-table, texture mapping.

1. INTRODUCTION

Various optical methods, such as stereo vision,[1–3] laser stripe scanning, structured light,[4,5] and digital fringe projection and phase shifting[6,7] have been developed in the past for 3D shape measurement. Compared to the other methods, the digital fringe projection and phase-shifting method has the advantage of high resolution and high measurement speed.

Phase-shifting methods have long been used in metrology for shape measurement. The measurement accuracy is usually affected by such error sources as the phase shift error,[8–10] non-sinusoidal waveforms,[11] camera noise and nonlinearity,[12] vibration,[13] speckle noise,[14] etc. In the digital fringe projection and phase-shifting method, which uses a digital video projector to generate the phase-shifted fringe patterns, non-sinusoidal waveform is the single dominant error source. It results from the nonlinearity of the gamma curve of the projector and can cause significant phase measurement error. Previously proposed methods, such as the double three-step phase-shifting algorithm,[15] the 3+3 phase-shifting algorithm,[16,17] and the direct correction of the nonlinearity of the projector's gamma curve,[6] were successful in significantly reducing the phase measurement error, but the residual error remains non-negligible. In this research, we propose a novel phase error compensation method that can produce significantly better results. This method is developed based on our finding that the phase error due to non-sinusoidal waveform depends only on the nonlinearity of the projector's gamma curve. Therefore, if the projector's gamma curve is calibrated and the phase error due to the nonlinearity of the gamma curve is calculated, a look-up-table (LUT) that stores the phase error can be constructed for error compensation. In addition to phase error compensation, a similar method is also proposed to correct the non-sinusoidality of the

---

When this work was done, Song Zhang was with the Department of Mechanical Engineering, SUNY at Stony Brook.

fringe patterns for the purpose of generating a more accurate flat image of the object for texture mapping, which is important for applications in computer vision and computer graphics.

The rest of the paper is organized as follows: Section 2 introduces the theoretical background of the proposed method, Section 3 and Section 4 show some simulation and experimental results, and Section 5 concludes the paper.

2. PRINCIPLE

2.1. Three-step phase-shifting algorithm

Phase-shifting method has been used extensively in optical metrology to measure 3D shapes of objects at various scales. In this method, a series of phase-shifted sinusoidal fringe patterns are recorded, from which the phase information at every pixel is obtained. This phase information helps determine the correspondence between the image field and the projection field. Once this correspondence is determined, the 3D coordinate information of the object can be retrieved based on triangulation.

Many different phase-shifting algorithms have been developed. In this research, a three-step phase-shifting algorithm is used,[18] which requires three phase-shifted images. The intensities of the three images with a phase shift of $2\pi/3$ are as follows:

$$I_1(x,y) = I'(x,y) + I''(x,y)\cos[\phi(x,y) - 2\pi/3], \tag{1}$$

$$I_2(x,y) = I'(x,y) + I''(x,y)\cos[\phi(x,y)], \tag{2}$$

$$I_3(x,y) = I'(x,y) + I''(x,y)\cos[\phi(x,y) + 2\pi/3], \tag{3}$$

where $I'(x,y)$ is the average intensity, $I''(x,y)$ is the intensity modulation, and $\phi(x,y)$ is the phase to be determined. Solving Eqs.(1)–(3) simultaneously, we obtain

$$\phi(x,y) = \arctan\left(\sqrt{3}\frac{I_1 - I_3}{2I_2 - I_1 - I_3}\right), \tag{4}$$

$$I'(x,y) = \frac{I_1 + I_2 + I_3}{3}, \tag{5}$$

$$I''(x,y) = \frac{[3(I_1 - I_3)^2 + (2I_2 - I_1 - I_3)^2]^{1/2}}{3}, \tag{6}$$

$$\gamma(x,y) = \frac{I''(x,y)}{I'(x,y)} = \frac{[3(I_1 - I_3)^2 + (2I_2 - I_1 - I_3)^2]^{1/2}}{I_1 + I_2 + I_3}. \tag{7}$$

Here $\phi(x,y)$ is the so-called modulo 2π phase at each pixel whose value ranges from 0 to 2π. If the fringe patterns contain multiple fringes, phase unwrapping[19] is necessary to remove the sawtooth-like discontinuities and obtain a continuous phase map. Once the continuous phase map is obtained, the phase at each pixel can be converted to xyz coordinates of the corresponding point through calibration.[20, 21] The average intensity $I'(x,y)$ represents a flat image of the measured object and can be used for texture mapping in computer vision and graphics applications. $\gamma(x,y)$, which has a value between 0 and 1, is called data modulation and can be used to determine the quality of the phase data at each pixel with 1 being the best.

In this research, the three-step algorithm is implemented in a real-time 3D shape measurement system.[7] The three phase-shifted fringe patterns are created in the R, G, and B channels of a computer-generated color image, but projected to the object as grayscale fringe patterns by a digital video projector working in a black-and-white mode.
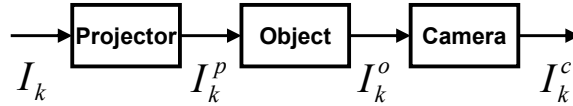
Figure 1. Fringe image generation procedure.

2.2. Phase error compensation

The images captured by the camera are formed through the procedure illustrated in Figure 1. Without loss of generality, we consider only the case of the three-step phase-shifting algorithm with a phase shift of $2\pi/3$. Let us assume that the projector's input sinusoidal fringe patterns generated by a computer have the intensity as

$$I_k(x,y) = a_0 \left\{ 1 + \cos\left[\phi(x,y) + \frac{2(k-2)\pi}{3} \right] \right\} + b_0, \tag{8}$$

where $k = 1, 2, 3$, a_0 is the dynamic range of the fringe images, and b_0 is the bias. After being projected by the projector, the output intensity of the fringe patterns becomes

$$I_k^p(x,y) = f_k(I_k), \tag{9}$$

where $f_k(I_k)$ as a function of I_k represents the real projection response of the projector to the input intensity in channel k. If we assume that the projector projects light onto a surface with reflectivity $r(x,y)$ and that the ambient light that shines on the surface is $a_1(x,y)$, the reflected light intensity is

$$I_k^o(x,y) = r(x,y)[I_k^p(x,y) + a_1(x,y)]. \tag{10}$$

This reflected light is captured by a camera with a sensitivity of α, which is a constant if the camera is assumed to have a linear response to the input light intensity. The intensity of the image captured by the camera is then

$$I_k^c(x,y) = \alpha[I_k^o + a_2(x,y)], \tag{11}$$

where $a_2(x,y)$ represents the ambient light that enters the camera directly.

Based on the three-step phase-shifting algorithm, phase $\phi(x,y)$ can be calculated as follows:

$$
\begin{aligned}
\phi(x,y) &= \tan^{-1}\left(\sqrt{3}\frac{I_1^c - I_3^c}{2I_2^c - I_1^c - I_3^c} \right) \\
&= \tan^{-1}\left\{ \frac{\sqrt{3}\{\alpha\left[r(I_1^p + a_1) + a_2\right] - \alpha[r(I_3^p + a_1) + a_2]\}}{2\alpha[r(I_2^p + a_1) + a_2] - \alpha[r(I_1^p + a_1) + a_2] - \alpha[r(I_3^p + a_1) + a_2]} \right\} \\
&= \tan^{-1}\left(\sqrt{3}\frac{I_1^p - I_3^p}{2I_2^p - I_1^p - I_3^p} \right).
\end{aligned}
\tag{12}
$$

From this equation we can see that phase $\phi(x,y)$ is independent of the response of the camera, the reflectivity of the object surface, and the intensity of the ambient light. This indicates that the phase error due to non-sinusoidal waveforms depends only on the nonlinearity of the projector's gamma curve. Therefore if the projector's gamma curve is calibrated and the phase error due to the nonlinearity of the gamma curve is calculated, a LUT that stores the phase error can be constructed for phase error compensation.

The following steps describe the procedure of constructing such an LUT:

1. Measure the gamma curves of the projector. A series of gray scale images with different gray scale values I_n $(n = 1, 2, \cdots, N)$ are sent to the projector. The projector projects the gray scale images with intensity values $f_k(I_n)$ onto a white board. The reflected images are captured by the camera and the intensities at the center of the images, I_{kn}^c, are calculated and recorded. Figure 2 shows a typical example of the measured gamma curves for R, G, and B channels. It is obvious that the curves are nonlinear and unbalanced.
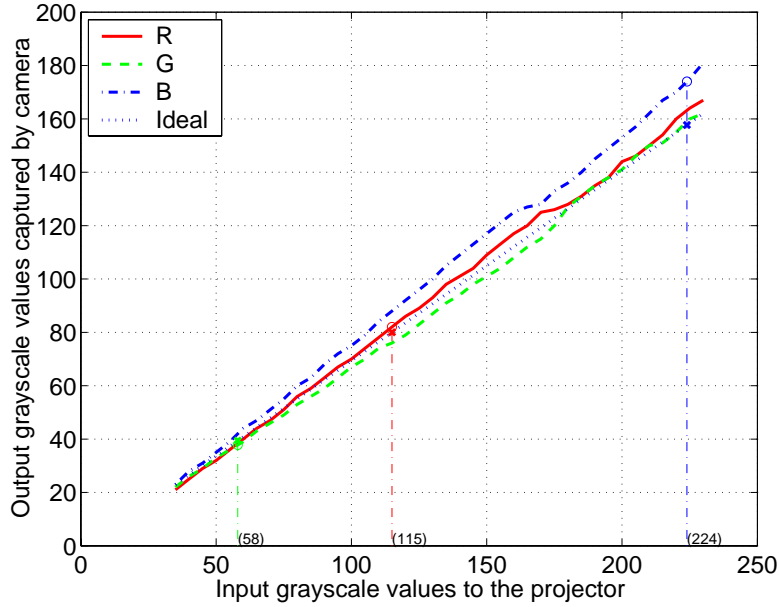
Figure 2. Measured gamma curves of the projector.

2. Fit the measured gamma curves with spline curves to obtain the gamma curve functions $f_k(I)$.

3. Use the gamma curve functions $f_k(I)$ to simulate fringe projection and phase shifting. Calculate the phase ϕ using Eq. (12) as well as the phase error $\Delta\phi$, which is the difference between this phase and the ideal phase.

4. Store the phase and phase error $(\phi, \Delta\phi)$ in an LUT for phase error compensation.

The constructed phase error LUT can be used to significantly reduce phase errors in real measurements. Since it depends only on the gamma curves of the projector, this LUT can be constructed once for all as long as the gamma curves are not changed. The same method can be applied to correct non-sinusoidal fringe images, which is important for applications that require high quality texture maps, as is discussed in the following section.

2.3. Texture mapping

In theory the texture map of the object can be generated by simply averaging the three phase-shifted fringe images with $2\pi/3$ of phase shift. However, if the fringe images are not exactly sinusoidal due to, for example, nonlinearity of the gamma curves, the texture map generated by simple averaging will show residual fringes, which is not desirable for high quality texture mapping. In this research, we found that the non-sinusoidal fringe images could be corrected by solving a reverse problem.

From previous discussions, we know that $(\phi, f_k(I))$ forms a one-to-one map when $\phi \in [0, 2\pi)$ and that $f_k(I)$ is monotonous and invertible. Therefore, for a given phase value ϕ ranging from 0 to 2π, its corresponding points $(I_k, f_k(I_k))$ on the gamma curves can be uniquely determined. Now Let us define an ideal gamma curve $\hat{f}(I)$, which is a straight line, for all channels with the starting and ending points defined as follows:

$$\hat{f}(I_1) = \max\{f_k(I_1)\},\tag{13}$$

$$\hat{f}(I_N) = \min\{f_k(I_N)\}.\tag{14}$$

Then the corresponding points of the same ϕ on the ideal gamma curve $(I_k, \hat{f}(I_k))$ can also be uniquely determined. This means that the ratio

$$R_k = \frac{f_k(I_k)}{\hat{f}(I_k)}\tag{15}$$

which we call gamma ratio, is uniquely defined for any given ϕ. Therefore, we can build a gamma ratio LUT (ϕ, R_k) to first correct the non-sinusoidal fringe images and then produce the texture map by averaging the fringe images.

The following steps describe the procedure of constructing such an LUT:

1. Follow the Steps 1–3 in the procedure of constructing the phase error LUT to find the phase value ϕ.

2. Find the ideal gamma curve function $\hat{f}(I)$ based on the definition in Eqs. (13) and (14).

3. Find the corresponding points of each phase value ϕ on the three gamma curves $(I_k, f_k(I_k))$ as well as the ideal gamma curve $(I_k, \hat{f}(I_k))$.

4. Calculate the gamma ratio R_k and store (ϕ, R_k) in an LUT for fringe image correction.

To explain how this gamma ratio LUT can be used to correct the non-sinusoidal fringe images and make them sinusoidal, we use an example for the case when the phase value is $\pi/4$. The corresponding points of this phase value on the measured R, G, and B gamma curves are $(115, 82.00)$, $(58, 37.80)$, and $(224, 174.00)$ respectively, as shown in Figure 2. The ideal gamma curve is

$$\hat{f}(I) = \frac{162 - 23}{230 - 35}(I - 35) + 23. \tag{16}$$

Using this equation, we can calculate the grayscale values of the corresponding points on the ideal gamma curve and they are $(115, 80.03)$, $(58, 39.39)$, and $(224, 157.72)$, respectively. The gamma ratios are then calculated according to Eq. (15) as

$$\{(0.9760, 1.0421, 0.9064)|\phi = \pi/4\}.$$

These gamma ratio values are stored in the gamma ratio LUT and used in real measurement to correct the grayscale values of the fringe images at any pixel whose phase value is $\phi = \pi/4$. After the fringe images are corrected to be ideally sinusoidal, we can then average these images to generate the flat image of the object for high quality texture mapping.

3. SIMULATION RESULTS

As shown in Figure 2, typical gamma curves for the projector we used have usable grayscale values ranging from 35 to 235. Beyond this range, the gamma curves are almost flat and cannot be used. As a simulation, we use these gamma curves to generate three phase shifted fringe patterns with a phase shift of $2\pi/3$ in the projector's red, green, and blue color channels, respectively. The input fringe patterns are as follows:

$$I_k(x, y) = 100 \left\{ 1 + \cos \left[\frac{2\pi x}{p} + \frac{2(k-2)\pi}{3} \right] \right\} + 35, \tag{17}$$

where $k = 1, 2, 3$ represent the three color channels and p is the fringe pitch used. By using the gamma curves, we can simulate the fringe patterns after these input fringe patterns are projected by the projector. Figure 3(a) shows the cross sections of the simulated fringe patterns. After the fringe correction algorithm is applied, the cross sections of the same fringe patterns are shown in Figure 3(b). It is clear that after the correction, the fringe patterns become more sinusoidal in shape and also better balanced between the three patterns in terms of intensity.

If we use the simulated fringe patterns before correction to compute the phase map directly, the phase error is approximately 2.4%, as shown in Figure 4(a). After phase error compensation using the constructed phase error LUT, the phase error is reduced to 0.2% as shown in Figure 4(b). Correcting the fringe or the phase does not make any difference in simulation. However, for real captured images, they are slightly different due to the existence of the ambient light, $a_1(x, y)$ and $a_2(x, y)$, which will be explained in the next section.

(a)   (b)
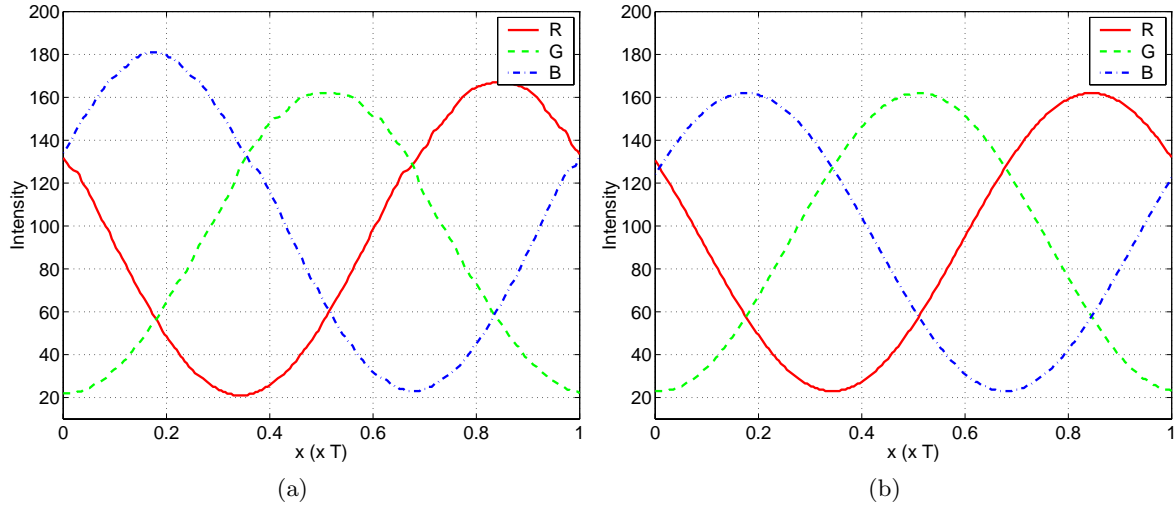
Figure 3. Cross sections of simulated fringe patterns before and after correction. (a) Cross sections of fringe patterns before correction. (b) Cross sections of fringe patterns after correction.


(a) Phase error before compensation   (b) Phase error after compensation
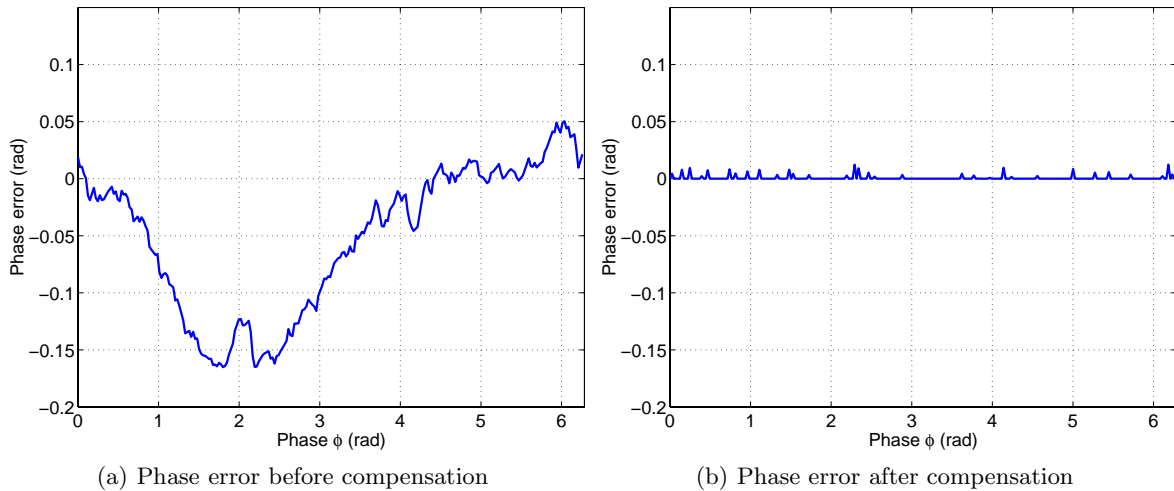
Figure 4. Phase error before and after phase error compensation.

4. EXPERIMENTAL RESULTS

Our simulation results show that we can use LUTs to reduce phase error and correct fringe images. To verify that this method works in real systems, we implemented the algorithms in our real-time 3D shape measurement system.[7] We first measured a flat board. The result is shown in Figure 5. Figure 5(a) shows the cross sections of the acquired fringe images. The fringe patterns were projected by a projector with gamma curves shown in Figure 2. We see that the three fringe images are not well balanced. Figure 5(b) shows the cross sections of the fringe images after correction, which are more balanced.

Figure 6 shows a comparison of the reconstructed 3D results before and after fringe or phase correction. It is clear that correcting the phase error directly results in higher accuracy than correcting fringe images. We believe this difference is due to the existence of ambient light $a_1(x, y)$ and $a_2(x, y)$. The texture maps before and after fringe correction are shown in Figure 7. The texture map before correction shows vertical stripes. After the correction, the stripes are barely seen and the image quality is sufficient for texture mapping purpose.

We also measured a plaster head model. Figure 8 shows the reconstructed 3D geometry before and after fringe
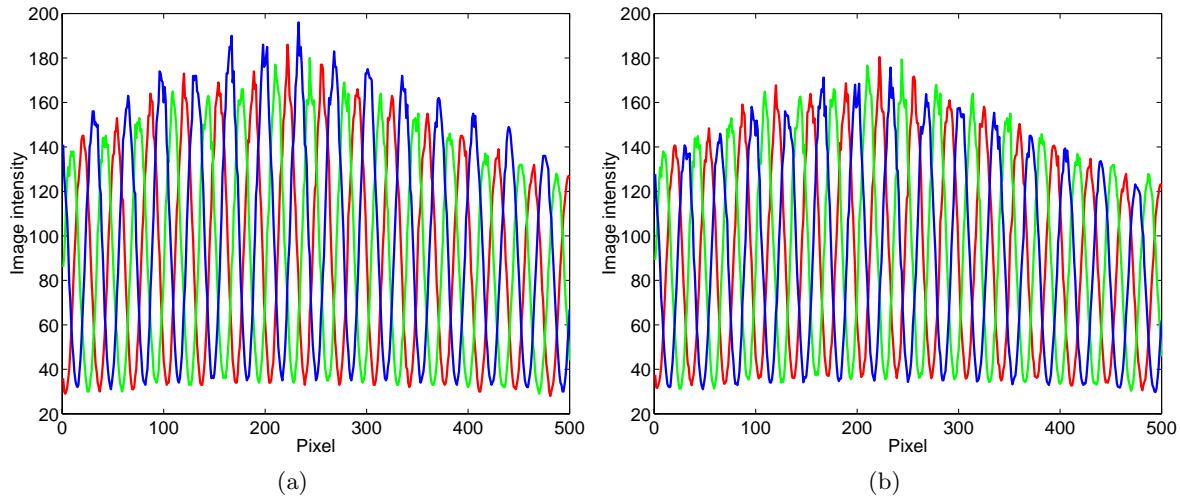
Figure 5. Fringe correction for real captured fringe images. (a) Cross sections of the fringe images before correction. (b)Cross sections of the fringe images after correction.

or phase correction. The reconstructed 3D geometric surface after phase correction or phase error compensation is very smooth. Figure 8(a) shows the reconstructed 3D geometry before fringe or phase correction. Figure 8(b) shows the 3D geometry reconstructed by using the compensated fringe images. Figure 8(c) shows the 3D geometry after correcting phase error directly. Figure 8(d) is the 3D result with corrected texture mapping. These experimental results confirmed that the error correction algorithms improved the accuracy of measurement and reduced stripe patterns in the texture image.

5. CONCLUSIONS

This paper introduced a novel phase error compensation method for a 3D shape measurement system based on the phase-shifting method. In this 3D shape measurement system, the phase-shifted fringe patterns are generated by a video projector. The main error source of this system is the nonlinearity of the projector's gamma curves, which results in non-sinusoidal waveforms in the fringe patterns and causes phase error in the measurement. Our analysis showed that phase error in the measurement is caused only by the nonlinearity of the projector's gamma curves. Therefore, to eliminate the phase error, we proposed a phase error compensation method that uses an LUT to store the phase error calculated based on the calibrated gamma curves of the projector. Our experimental results demonstrated that by using the proposed method, the measurement error could be reduced by 10 times. In addition to phase error compensation, a similar LUT method was also proposed to correct the non-sinusoidality of the fringe patterns for the purpose of generating a more accurate flat image of the object for texture mapping.

ACKNOWLEDGMENTS

REFERENCES

1. U. Dhond and J. Aggarwal, "Structure from stereo-a review," *IEEE Trans. Systems, Man, and Cybernetics* **19**(6), pp. 1489–1510, 1989.
2. L. Zhang, B. Curless, and S. Seitz, "Spacetime stereo: Shape recovery for dynamic senses," in *Proc. Copmuter Vison and Pattern Recognition*, 2003.
3. J. Davis, R. Ramamoorthi, and S. Rusinkiewicz, "Spacetime stereo: A unifying framework for depth from triangulation," *IEEE Trans. on Pattern Analysis and Machine Intelligence* **27**(2), pp. 1–7, 2005.
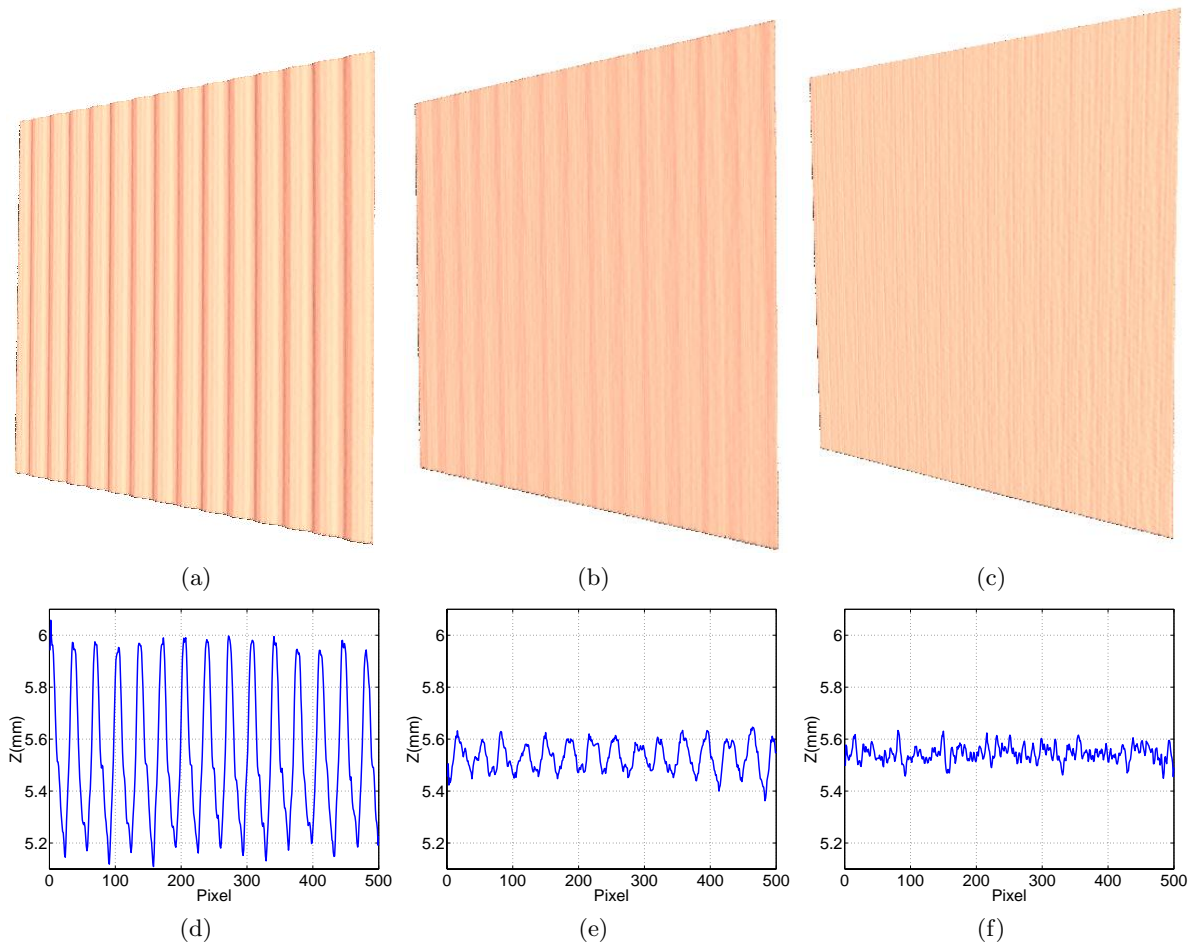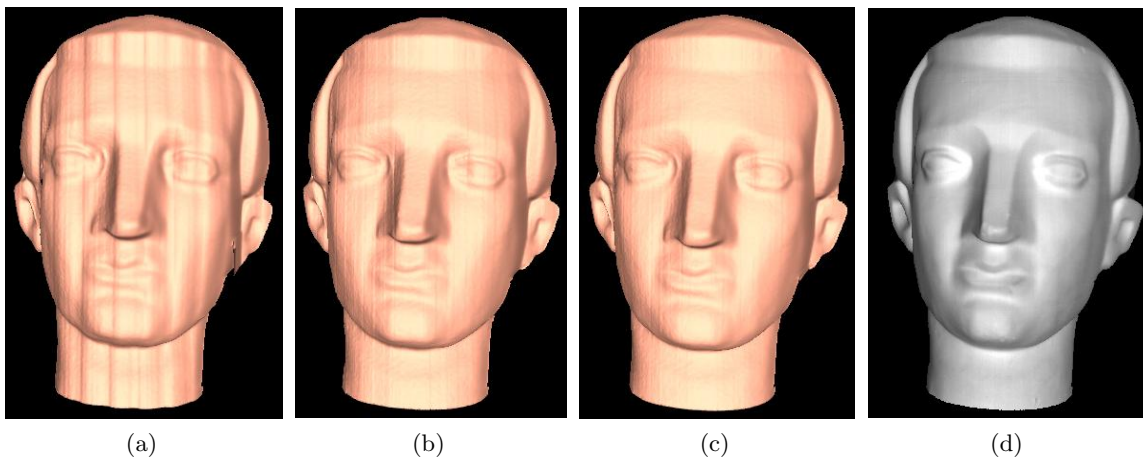
Figure 6. Reconstructed 3D geometries of a flat board before and after fringe or phase correction. (a) 3D geometry before correction. (b) 3D geometry after fringe correction. (c) 3D geometry after phase correction. (d)-(f) Cross sections of the corresponding 3D geometries in (a)-(c).

4. J. Salvi, J. Pages, and J. Batlle, "Pattern codification strategies in structured light systems," *Pattern Recognition* **37**(4), pp. 827–849, 2004.

5. R. A. Jarvis, "A perspective on range finding techniques for computer vision," *IEEE Trans. Pattern Analysis and Machine Intelligence* **5**(2), pp. 122–139, 1983.

6. P. S. Huang, C. Zhang, and F. P. Chiang, "High-speed 3-d shape measurement based on digital fringe projection," *Opt. Eng.* **42**(1), pp. 163–168, 2003.

7. S. Zhang and P. Huang, "High-resolution, real-time dynamic 3-d shape acquisition," in *IEEE Computer Vision and Pattern Recognition Workshop (CVPRW'04)*, **3**(3), pp. 28–37, 2004.

8. J. Schwider, T. Dresel, , and B. Manzke, "Some considerations of reduction of reference phase error in phase-stepping interferometry," *Appl. Opt.* **38**, pp. 655–658, 1999.

9. C. Joenathan, "Phase-measuring interferometry: New methods and error analysis," *Appl. Opt.* **33**, pp. 4147–4155, 1994.

10. P. Hariharan, "Phase-shifting interferometry: minimization of system errors," *Appl. Opt.* **39**, pp. 967–969, 2000.

11. K. Hibino, B. F. Oreb, D. I. Farrant, and K. G. Larkin, "Phase shifting for nonsinusoidal waveforms with phase-shift errors," *J. Opt. Soc. Am. A.* **12**(4), pp. 761–768, 1995.
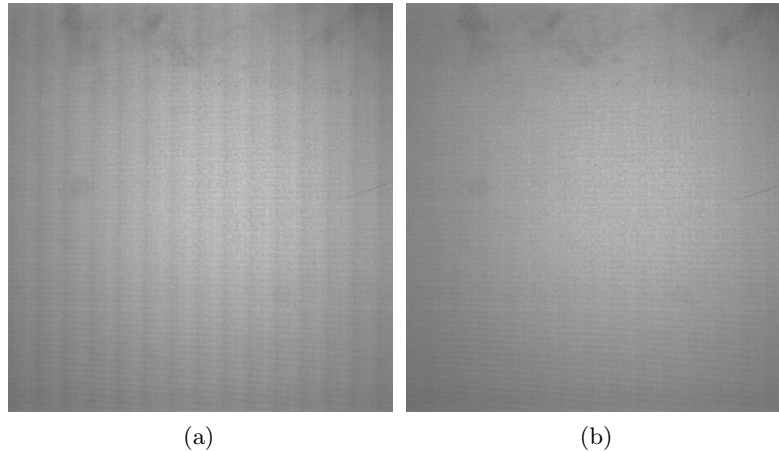
Figure 7. Texture maps before and after fringe correction. (a) Texture map before fringe correction. (b) Texture map after fringe correction.

Figure 8. Reconstructed 3D geometries of the head model before and after fringe or phase correction. (a) 3D geometry before correction. (b) 3D geometry after fringe correction. (c) 3D geometry after phase correction. (d) 3D geometry with corrected texture mapping.

12. T. Maack and R. Kowarschik, "Camera influence on the phase measuring accuracy of a phase-shifting speckle interferometry," *Appl. Opt.* **35**(19), pp. 3514–3524, 1996.

13. P. L. Wizinowich, "Phase-shifting interferometry in the presence of vibration: a new algorithm and system," *Appl. Opt.* **29**(22), pp. 3266–3279, 1990.

14. B. Trolard, C. Gorecki, and G. M. Tribillon, "Speckle noise removal in interference fringes by optoelectronic preprocessing with epson liquid crystal television," in *Proc. of SPIE: in Laser Interferometry VIII: Techniques and Analysis*, **2860**, pp. 126–134, 1996.

15. P. S. Huang, Q. Y. Hu, , and F. P. Chiang, "Double three-step phase-shifting algorithm," *Appl. Opt.* **41**(22), pp. 4503–4509, 2002.

16. J. Schwider, R. Burow, J. Elssner, K. E. abd Grzanna, R. Spolaczyk, and K. Merkel, "Digital wave-front measuring interferometry: Some systematic error sources," *Appl. Opt.* **22**, pp. 3421–3432, 1983.

17. J. C. Wyant and K. N. Prettyjohns, "Optical profiler using improved phase-shifting interferometry," 1987. U.S. Pat. 4,639,139.

18. D. Malacara, ed., *Optical Shop Testing*, John Wiley and Songs, NY, 1992.

19. D. C. Ghiglia and M. D. Pritt, *Two-Dimensional Phase Unwrapping: Theory, Algorithms, and Software*, John Wiley and Sons, Inc, 1998.

20. R. Legarda-Sáenz, T. Bothe, and W. P. Jüptner, "Accurate procedure for the calibration of a structured light system," *Opt. Eng.* **43**(2), pp. 464–471, 2004.

21. Q. Hu, P. S. Huang, Q. Fu, , and F. P. Chiang, "Calibration of a 3-d shape measurement system," *Opt. Eng.* **42**(2), pp. 487–493, 2003.